EES Catalysis

PAPER

View Article Online
View Journal | View Issue



Cite this: *EES Catal.*, 2025, 3, 756

# DBD plasma-thermal tandem reactors for converting biogas to carbon nanofibers†

Kevin K. Turaczy,[a] Zhenhua Xie[ab] and Jingguang G. Chen *[ab]

Received 15th January 2025,
Accepted 15th May 2025

DOI: 10.1039/d5ey00009b

rsc.li/eescatalysis

Sequestering greenhouse gases ($CO_2$ and $CH_4$) in biogas into carbon nanofibers (CNF) offers a promising route to mitigate carbon emissions and create value-added solid carbon materials. Coupling non-thermal plasma with a thermocatalytic reactor in a tandem setup is a promising approach for tandem reactions of dry reforming of methane to synthesis gas and its subsequent conversion to CNF. Various parameters were studied to determine their effects on CNF growth. Decreasing the total flow rate resulted in an increase in CNF growth. Increasing the plasma power input or the plasma zone length also enhanced the production of CNF. These results illustrate that plasma-thermal tandem reactors can be used to synthesize CNF from biogas with tunable parameters that may be further optimized in future studies.

**Broader context**

Biogas, a mixture of primarily methane ($CH_4$) and carbon dioxide ($CO_2$), is a sustainable resource that originates from the decomposition of organic matter. The unabated release of these greenhouse gases (GHG) contributes towards anthropogenic climate change. Conversion of biogas into solid materials presents an alternative abatement strategy for biogas that can permanently sequester these GHG. Carbon nanofibers (CNF) are high-value materials that have applications in gas storage, composites, energy conversion devices, and catalysis. Biogas conversion to CNF consists of the dry reforming of methane (DRM) to syngas and subsequent conversion to CNF. The difference in thermodynamic favorability between these two steps results in equilibrium limitations if carried out in a single reactor. A tandem reactor that isolates each step can be used to circumvent these limitations; however, the DRM relies on high reaction temperatures. In this work, non-thermal plasma is used to convert biogas into syngas at near-atmospheric temperatures and is coupled with a thermocatalytic reactor to achieve CNF production from biogas.

## Introduction

Biogas, a mixture of primarily methane ($CH_4$) and carbon dioxide ($CO_2$), is a sustainable resource that originates from the decomposition of organic matter. Both $CO_2$ and $CH_4$, which has a global warming potential 27–34 times higher than $CO_2$, are released from prevalent sources such as crop residue and animal manure. Therefore, capturing these greenhouse gases would aid in the effort to mitigate climate change.[1] At present less than 10% of biogas feedstocks are used, and the availability of these feedstocks is expected to increase by 40% by 2040 resulting in unabated biogas entering the atmosphere.[2] Extracted biogas is primarily burned for heat and electricity generation. Some biogas is upgraded to biomethane by removing $CO_2$, which can account for as much as 50% depending on the biogas source.[3] Though biomethane can be used as a substitute for conventional natural gas with a higher heating value than raw biogas, the energy and cost associated with its separation reduces the overall impact of using biomethane, instead of natural gas, as a feedstock. Biogas utilization strategies that can sequester both $CH_4$ and $CO_2$ are therefore attractive alternatives for preventing these greenhouse gases from being released into the atmosphere.

One such possible route is converting biogas into solid carbon nanomaterials. Carbon nanomaterials (CNM) include many variations such as nanotubes (CNT), graphene, and nanofibers (CNF), which have a wide range of applications.[4–6] CNF specifically can be used in composites, energy conversion devices, gas storage, and as a catalyst support material.[7–12] Previous studies of biogas conversion typically utilize high reactor temperatures ($T \geq 600$ °C) and the addition of a catalyst, typically nickel-based, to promote the dry reforming of methane (DRM) (**R1**).[13–15] With the formation of syngas *via* DRM, pathways **R2** and **R3** can further lead to CNF synthesis. The difference in thermodynamic favorability between **R1** (endothermic) and **R2**

[a] *Department of Chemical Engineering, Columbia University, New York, NY, 10027, USA. E-mail: jgchen@columbia.edu*
[b] *Chemistry Division, Brookhaven National Laboratory, Upton, NY, 11973, USA*

† Electronic supplementary information (ESI) available. See DOI: https://doi.org/10.1039/d5ey00009b

& **R3** (exothermic) reactions, however, leads to equilibrium limitations if carried out in a conventional single reactor. To circumvent restrictions imposed by using a single reactor, tandem reactors have been proposed as a method that can optimize the individual steps of an overall process for $CO_2$ conversion.[16–19] In a recent work we demonstrated the feasibility of using a thermochemical-thermochemical tandem process for converting biogas to CNF.[16] We also performed $CO_2$ footprint analysis, which suggested the potential benefits of using a plasma-thermocatalytic tandem reactor. We also provided preliminary results to demonstrate the feasibility of coupling non-thermal plasma with a thermocatalytic reactor in a tandem setup for CNF synthesis from biogas.[16] In the current work we varied different parameters, including the total flow rate of the biogas, the $CO_2$/$CH_4$ ratio in the feed, the plasma zone length, and the plasma power to determine their effects on CNF growth using the plasma-thermocatalytic tandem reactor.

Non-thermal plasma is an amalgam of ions, radicals, and excited species that operates under non-equilibrium conditions allowing for high energy electrons (1–10 eV) to facilitate reactions while the bulk gas remains at near-atmospheric temperature and pressure. A non-thermal plasma is generated by creating a high voltage difference across a dielectric (dielectric barrier discharge, DBD), such as a feed gas, allowing for integration of renewable electricity. Since non-thermal plasma can be instantaneously switched on/off, utilizing a plasma-thermal tandem setup would allow for easier maintenance on the plasma module that could be quickly reintegrated into the process. In this study, non-thermal plasma is used to convert biogas into syngas in a flow reactor where the effluent is fed into a thermal reactor to generate CNF. Unlike in a thermal reactor where very high temperatures ($T \geq$ 800 °C) would typically be required for $CH_4$ decomposition (**R4**), the non-thermal plasma approach is attainable without added heat given the high electronic temperature present in the plasma. The generation of $H_2$ from **R4**, coupled with the generation of CO from plasma-driven $CO_2$ dissociation (**R5**), could promote CNF formation *via* **R3**. The production of $H_2$ in the plasma can also promote more CO generation *via* **R6** followed by the Boudouard reaction (**R2**) to generate CNF. Previous works have demonstrated that DBD plasma is capable of DRM; however, it has yet to be seen how a $CH_4$/$CO_2$ DBD plasma can be tuned for CNF production.[20–23] The current study is aimed to determine the effect of plasma on CNF growth in plasma-thermal tandem reactors.

**R1:** $CH_4 + CO_2 \rightleftharpoons 2CO + 2H_2 \quad \Delta H_{rxn,298K} = 247\ kJ\ mol^{-1}$.

**R2:** $2CO \rightleftharpoons C(s) + CO_2 \quad \Delta H_{rxn,298K} = -172\ kJ\ mol^{-1}$.

**R3:** $CO + H_2 \rightleftharpoons C(s) + H_2O \quad \Delta H_{rxn,298K} = -131\ kJ\ mol^{-1}$.

**R4:** $CH_4 \rightleftharpoons C(s) + 2H_2 \quad \Delta H_{rxn,298K} = 76\ kJ\ mol^{-1}$.

**R5:** $CO_2 \rightleftharpoons CO + O \quad \Delta H_{rxn,298K} = 532\ kJ\ mol^{-1}$.

**R6:** $CO_2 + H_2 \rightleftharpoons CO + H_2O \quad \Delta H_{rxn,\ 298K} = 41\ kJ\ mol^{-1}$.

# Experimental methods

### Catalyst synthesis

The $Co_{12}K_5/CeO_2$ (Co wt% = 6.0) catalyst was synthesized using a slurry co-impregnation method where appropriate amounts of cobalt(II) nitrate hexahydrate (99.999% trace metal basis, Sigma-Aldrich) and potassium nitrate (ReagentPlus®, ≥99.0%, Sigma-Aldrich) were dissolved in 30 mL of DI water. This was followed by ultrasonication for 5 min. The $CeO_2$ support (35–45 $m^2\ g^{-1}$, Sigma-Aldrich) was slowly added to the suspension under rigorous stirring. The suspension was heated at 70 °C overnight until dry, followed by calcination at 400 °C in static air for 2 h with a ramp rate of 1 °C $min^{-1}$. For the $Ni_4Fe/\gamma$-$Al_2O_3$ catalyst, $\gamma$-$Al_2O_3$ particles (80–120 $m^2\ g^{-1}$, Alfa-Aesar) were sieved using a 40–60 mesh tray (250–425 μm) before using a slurry co-impregnation method to introduce the $Ni_4Fe$ bimetallic. The atomic ratio of Ni : Fe used was 4 : 1 with a combined $Ni_4Fe$ loading of 10 wt%. Appropriate amounts of nickel(II) nitrate hexahydrate (puratronic, 99.9985% metal basis, Alfa-Aesar) and iron(III) nitrate nonahydrate (99.999% metal basis, Sigma-Aldrich) were dissolved in 30 mL of DI water, followed by 5 min of ultrasonication. The $Al_2O_3$ support was slowly added to the suspension under vigorous stirring. The $Ni_4Fe$ catalyst was then treated using the same heating and drying method as the $Co_{12}K_5$ catalyst. For benchmark experiments, $\gamma$-$Al_2O_3$ particles were similarly sieved before being loaded into the plasma zone of the quartz tube.

### Plasma-thermal tandem reactor

The effects of flow rate, molar feed ratio, input power, plasma zone length, and plasma catalyst on CNF growth within the coupled plasma-thermal reactor were investigated. Fig. 1 illustrates the plasma-thermal tandem reactor setup where one continuous quartz tube (ID: 4.35 mm, OD: 6 mm) housed both the plasma and thermal reactors. Reactants first passed through a DBD plasma (plasma reactor) and then passed through a tube furnace (thermal reactor). In the center of the tube furnace (Thermo Scientific, Lindberg Blue M), or thermal zone, 50 mg of $Co_{12}K_5/CeO_2$ was used to facilitate the conversion of syngas to CNF. A recent study reported $Co_{12}K_5/CeO_2$ to be an effective catalyst for CNF growth where K-modification was found to be important for CO activation and suppressing the reaction of CNF and $H_2$ to produce $CH_4$.[16] The catalyst was loosely distributed between two pieces of quartz wool (1.5 cm spacing) in order to reduce significant pressure buildup following CNF growth. The distance from the center of the thermal catalyst to the end of the plasma zone was 18 cm. Prior to each experiment, the catalyst in the thermal reactor was heated to 500 °C, at a ramp rate of 10 °C $min^{-1}$, and held for 1 h under an Ar/$H_2$ (20/20 mL $min^{-1}$) environment. The thermal reactor was then cooled to 450 °C under the same Ar/$H_2$ environment. A mixture of Ar/$CH_4$/$CO_2$ was then fed into this tandem reactor at a ratio of 5/3/2 mL $min^{-1}$. The effect of flow rate was investigated by varying the total flow rate but maintaining the molar ratio of reactants. The effect of feed molar ratio was measured by maintaining the total flow rate but varying the molar ratio of Ar/$CH_4$/$CO_2$.

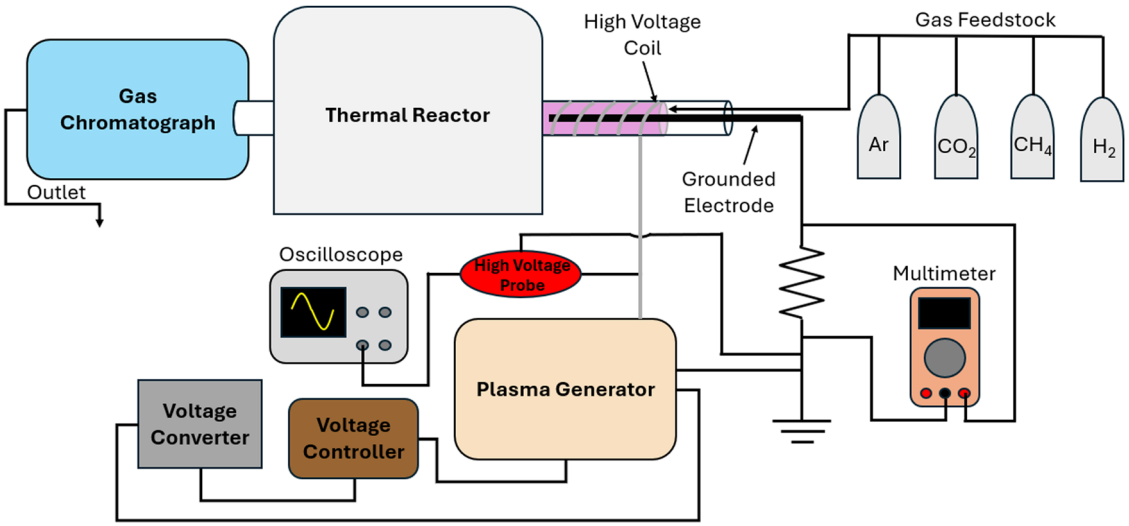


Fig. 1 Diagram of plasma-thermal tandem reactor setup.

At the start of each experiment, a DBD plasma was generated with an input power of 8 W ($f$ = 8–9 kHz) and a plasma zone length of 8 cm. This was done using a plasma generator (CTP-2000 K) connected to a voltage converter (Seyas, AT-1000) and coupled with a variable voltage controller. A tantalum coil wrapped around the quartz tube and a grounded K-type thermocouple ($D$ = 1 mm) were used as the high voltage and ground electrodes, respectively. In the case where a catalyst was introduced into the plasma zone, the catalyst was packed downstream of the plasma zone and occupied a length of 2 cm. This catalyst was reduced simultaneously with the thermal catalyst prior to an experiment. Each experiment lasted 5 hours during which the plasma operated at a constant power input and the thermal reactor operated at 450 °C. Effluent from the tandem reactor was analyzed using gas chromatography (Agilent 7890B) where Ar served as the internal standard. The gaseous product selectivity was calculated using eqn (1) where $S_i$ is the selectivity of species $i$ and $N_i$ is the total molar amount of species $i$ after each experiment. The reactant conversion was calculated using eqn (2) where $X_i$ is the conversion of species $i$, $n_{i,\text{in}}$ is the molar flow rate of species $i$ fed into the reactor, and $n_{i,\text{out}}$ is the molar flow rate of species $i$ flowing out of the reactor.

$$S_i = \frac{N_i[\mu\text{mol}]}{\sum_i N_i[\mu\text{mol}]} \times 100\% \quad (1)$$

$$X_i = \frac{n_{i,\text{in}} - n_{i,\text{out}}}{n_{i,\text{in}}} \times 100\% \quad (2)$$

The approximate power used to generate the plasma was estimated using an oscilloscope and an external resistor. A high voltage probe (Fluke 80K-40) was connected on one end to the high voltage line from the plasma generator and to a digital oscilloscope (Agilent Technologies, DSO1052B) on the other end. The high voltage probe served as a large impedance to protect the oscilloscope from damage. The oscilloscope provided the voltage as a function of time from which the frequency could also be derived. The root mean square voltage, $V_{\text{rms}}$, was determined using eqn (3) where $V_{\text{max}}$ was the maximum observed voltage and $V_{\text{min}}$ was the minimum observed voltage. When determining $V_{\text{max}}$ and $V_{\text{min}}$, a conversion factor (1901), as provided by Fluke, was used to obtain the actual voltage applied. An external 10 Ω resistor was connected in series between the ground electrode and ground in order to measure the current. A digital multimeter (Fluke 87 True RMS Multimeter) provided the voltage ($V_{\text{res}}$) across the resistor from which the root mean square current through the circuit, $I_{\text{rms}}$, could be derived using Ohm's law. The product of $V_{\text{rms}}$ and $I_{\text{rms}}$ gave the power input, $P_{\text{rms}}$, for the DBD plasma. Sample data and power analysis are included in Fig. S1 and Table S1 (ESI†).

$$V_{\text{rms}} = \frac{V_{\text{max}} - V_{\text{min}}}{2\sqrt{2}} \quad (3)$$

Since CNF formation over the $Co_{12}K_5/CeO_2$ catalyst was expected to grow *via* a tip-growth mechanism and thus remain bound to the catalyst, catalyst weight gain (CWG), which is the weight gain of the thermal catalyst from CNF accumulation after each experiment, was used as a metric for the impact of each parameter. The formation of CNF was verified using a JEM-1400 transmission electron microscope (TEM) and an accelerating voltage of 120 kV. To prepare the sample for TEM measurements, the catalyst was ultrasonically dispersed in ethanol for 3 min, dripped onto a Lacey carbon film (300 mesh) supported on copper grids, and dried at room temperature.

## Results and discussion

Altering the characteristics of the feed gas, either by total flow rate or by feed molar ratio, was observed to affect CNF growth in the thermal zone as seen in Table 1. While a total flow rate of 10 mL $\text{min}^{-1}$ resulted in a catalyst weight gain (CWG) of 23.2 mg, doubling the total flow rate reduced the CWG to 5.5 mg. Halving the total flow rate, however, increased the CWG to 34.9 mg. This trend suggests that longer residence times of the inlet species promoted CNF formation. Residence

Table 1 Varying feed gas parameters and their effects on catalyst weight gain

| Total flow (mL $min^{-1}$), molar ratio ($CH_4$:$CO_2$) | Residence time (s) | CWG (mg) |
|---|---|---|
| 20, 1.5 | 3.4 | 5.5 |
| 10, 1.5 | 6.8 | 23.2 |
| 5, 1.5 | 13.5 | 34.9 |
| 10, 2 | 6.8 | 10.3 |
| 10, 0.5 | 6.8 | 27.4 |

Note: the residence time reported here was for the plasma zone.

time here is calculated by dividing the plasma reactor volume by the total feed gas flow rate. Bie *et al.* modeled the various pathways for $CH_4$ and $CO_2$ in a DBD reactor and found that increasing the residence time up to 20 seconds led to a steady increase of $H_2$ production, which is required for CNF production in the thermal zone *via* **R3**.[24]

The total feed gas flow rate was observed to affect both $CO_2$ and $CH_4$ conversion though the latter was seen to be more sensitive (Fig. 2a). While $CO_2$ conversion was only slightly affected when decreasing the residence time, there was a significant increase in conversion when the residence time doubled – from 17% to 27%. A much more significant change occurred in the $CH_4$ conversion with a reduction to ~19% at higher flow rates and an increase to an average of 44% when reducing the flow rate. Attributing a change in CWG to changes in either $CO_2$ or $CH_4$ conversion, however, is difficult because **R2** regenerates $CO_2$ in the thermal zone after CNF formation thereby reducing the measured $CO_2$ conversion. Therefore, CWG may have increased as the residence time increased due to a higher $CO_2$ dissociation rate in the plasma zone, promoting **R2** in the thermal zone, and/or a significantly higher conversion of $CH_4$ in the plasma zone lead to an increase in CWG *via* the otherwise

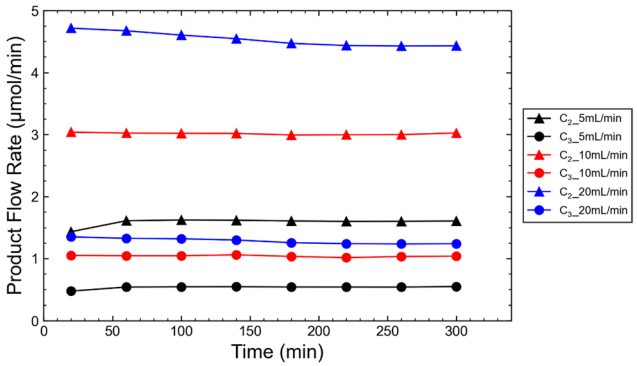


Fig. 3 Effect of total flow rate on $C_2$ (▲) and $C_3$ (●) species production. $C_2$ species included $C_2H_4$ and $C_2H_6$ while $C_3$ species included $C_3H_6$ and $C_3H_8$. Total flow rate was specified next to each dataset.

$H_2$-limited **R3** in the thermal zone. A difference in the morphology of CNF was also observed in TEM images where a lower total flow rate, or longer residence time, lead to longer CNF (Fig. 2b) compared to the shorter residence time which resulted in shorter and thinner CNF (Fig. 2d).

The generation of radicals in the plasma zone, specifically $CH_3$ radicals from the dissociation of $CH_4$ *via* electron impact, opens pathways to generating other hydrocarbons such as $C_2$ and $C_3$ species. The primary product of $CH_4$ consumption in a $CH_4/CO_2$ DBD plasma is $CH_3$, which is then almost entirely consumed to produce $C_2H_6$ and $C_3H_8$.[24] In the current study, the total production rate of $C_2$ and $C_3$ species increased as the residence time decreased (Fig. 3). Decreasing the residence time by a factor of 4 increased the selectivity of $C_{2+}$ products exiting the effluent stream by 50%. Moreover, the selectivity of $C_2H_4$ increased by over one order of magnitude and $C_3H_6$

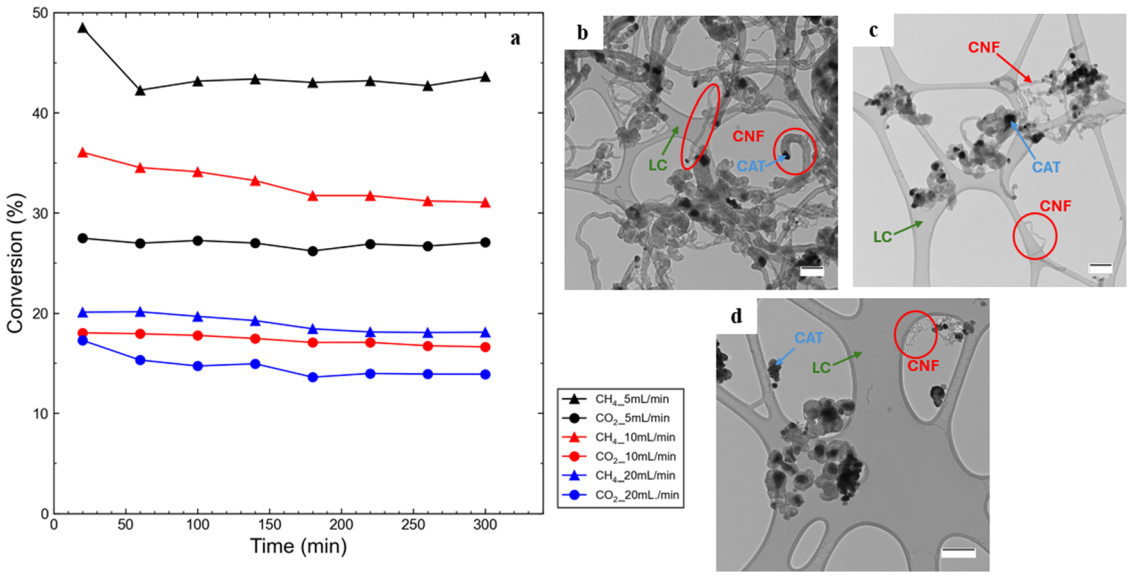


Fig. 2 (a) Conversion of $CH_4$ (▲) and $CO_2$ (●) over time during a 5 h experiment with Ar/$CH_4$/$CO_2$ ratio of 5/3/2 mL $min^{-1}$, 8 W input power, and 8 cm plasma zone length. Total flow rate was specified for each dataset. TEM images of $Co_{12}K_5/CeO_2$ after each trial for (b) 5 mL $min^{-1}$, (c) 10 mL $min^{-1}$, and (d) 20 mL $min^{-1}$ experiments. Indicators were included for examples of CNF (red), Lacey carbon (LC, green), and catalyst (CAT, blue) in the TEM images (b)–(d). Scale bar was 200 nm.

increased by a factor of 4 (Fig. S2, ESI†). The CWG, however, decreased and the $H_2$ selectivity in the effluent decreased with shorter residence times (Fig. 4).

Feed gas molar ratio was also seen to impact the CWG for the plasma-thermal tandem reactor. Increasing the $CH_4:CO_2$ molar ratio from 1.5 to 2 reduced the CWG from 23.2 mg to 10.3 mg. In addition, $CH_4$ and $CO_2$ conversion both decreased (Fig. S3, ESI†). Decreasing the $CH_4:CO_2$ ratio to 0.5 increased CWG, though not significantly. One possible reason for higher CWG seen with lower $CH_4:CO_2$ ratios is the increased presence of O radicals in the plasma zone, from $CO_2$ dissociation, that can go on to react with $CH_4$.[25] In fact, the $CO_2$-rich feed resulted in the highest selectivity of syngas amongst all trials in this work (Fig. 4). Decreasing the $CH_4:CO_2$ ratio from 2 to 1.5 did not affect the amount of $C_2$ and $C_3$ products despite increasing the CWG significantly (Fig. S4, ESI†).

The residence time that a reactant spends in the DBD plasma may also be altered by tuning the length of the plasma zone. To maintain the power density in the plasma zone, *i.e.*, power input per unit volume of plasma, the power was increased or decreased proportionally to the change in plasma zone length. The effect of plasma zone length is reported in Table 2 where a longer plasma zone length was seen to increase the downstream CWG. Similar to the effect of the total flow rate, the longer time a reactant spends in the plasma zone, the higher the probability it encounters a high energy electron or other reactive species. This was especially true for $CH_4$ as the conversion doubled from 28% to 59% as the plasma zone length increased from 4 cm to 11 cm (Fig. S5, ESI†), likely responsible for the increase in CWG from 11.2 mg to 53.1 mg. Examples of CNF growth for 8 cm and 11 cm plasma zone length experiments are shown in Fig. S6 (ESI†). This suggests that, along with reducing flow rates, lengthening the plasma zone can also serve as a way to increase the residence time of biogas species and increase CWG.

The effect of plasma power was investigated and CWG was observed to increase with increasing power input (Table 3). By increasing the power input, and maintaining the total flow rate, the specific energy input (SEI) (eqn (4)) was also increased. An increase in SEI is expected to increase the conversion of $CH_4$ and $CO_2$ since a higher power increases the number and energy of electrons in the plasma zone that are available to interact with the reactants.[26] As the SEI was increased from 24 J $mL^{-1}$ to 72 J $mL^{-1}$, the gas temperature also increased from 130 °C to 225 °C as measured by the ground electrode (thermocouple). Increasing the power input from 4 W to 12 W was seen to increase the $CH_4$ conversion by almost 2.5 times, from ~18% to ~44%. The conversion of $CO_2$ also showed a slight increase, from ~13% to 22%. Tripling the power input from 4 W to 12 W resulted in approximately double the amount of CWG.

$$\mathrm{SEI} = \frac{\text{Power input (W)}}{\text{Total flow rate (mL min}^{-1}\text{)}} \quad (4)$$

The CWG values from different plasma powers were used to estimate the apparent activation barrier for the conversion of biogas into CNF. The method is highlighted by Kim *et al.* and correlates the reaction rate with the SEI to estimate an apparent activation barrier for the reaction.[27] A linearization of this correlation is shown below (eqn (5)) where $dA/dt$ is the production rate of CNF from biogas (CWG), $E_A$ is the apparent activation barrier, and $b$ is a constant:

$$\ln\left(\frac{dA}{dt}\right) = -\left(\frac{E_A}{\mathrm{SEI}}\right) + b \quad (5)$$

Plotting the natural log of the CNF production rate as a function of the inverse power input resulted in a linear correlation (Fig. 5), which allowed for the determination of $E_A$ for the plasma-thermal reaction of biogas to CNF. A total flow rate of 10 mL $min^{-1}$ was used for all the experiments. An activation barrier of 700 kJ $mol^{-1}$, or 7.3 eV, was obtained, which is higher than that for non-catalytic DRM, 332 kJ $mol^{-1}$ or 3.4 eV.[28]

Similar to catalytic DRM, which can reduce activation barriers by an order of magnitude with catalysts, introducing a catalyst into the plasma zone is one possible way to reduce the activation barrier observed in the plasma-thermal tandem

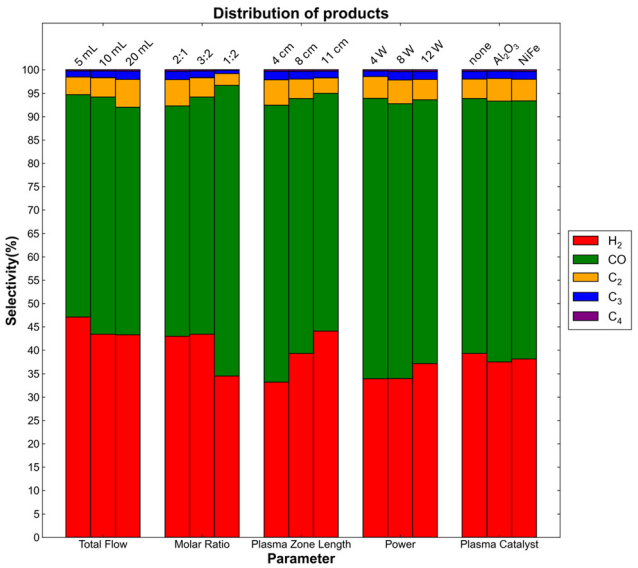


Fig. 4 Selectivity of gaseous products for all plasma-thermal trials. $C_2$ included $C_2H_4$ and $C_2H_6$, $C_3$ included $C_3H_6$ and $C_3H_8$, and $C_4$ included $C_4H_{10}$.

Table 2 The impact of plasma zone length on catalyst weight gain

| Plasma zone length (cm) | Residence time (s) | CWG (mg) |
|---|---|---|
| 4 | 3.4 | 11.2 |
| 8 | 6.8 | 34.2 |
| 11 | 9.3 | 53.1 |

Note: the residence time reported here was for the plasma zone.

Table 3 The effect of DBD plasma power input on catalyst weight gain

| Power input (W) | SEI (J $mL^{-1}$) | CWG (mg) |
|---|---|---|
| 4 | 24 | 19.2 |
| 6 | 36 | 30.2 |
| 8 | 48 | 33.7 |
| 12 | 72 | 43.5 |

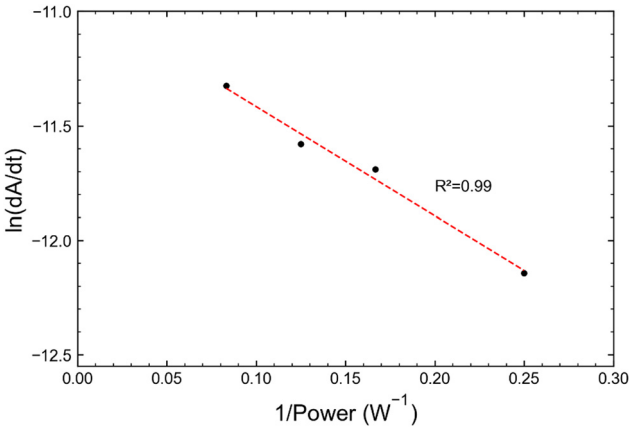


Fig. 5 Modified Arrhenius equation and linear fit for the plasma-thermal biogas conversion to CNFs.

Table 4 Impact of catalysts in the plasma zone on catalyst weight gain

| Plasma catalyst | CWG (mg) |
|---|---|
| None | 34.2 |
| $\gamma$-$Al_2O_3$ | 34.9 |
| $Ni_4Fe/Al_2O_3$ | 28.8 |

process. Previous studies have shown how Ni-based catalysts can be used for both thermal and plasma DRM to improve conversion.[29–31] A $Ni_4Fe/Al_2O_3$ catalyst, as well as a metal-free $\gamma$-$Al_2O_3$ reference, were tested inside the plasma zone to determine their effects on CNF growth. The former was chosen because $Ni_4Fe$ bimetallic was shown to promote DRM and limit coking deactivation,[32] while $\gamma$-$Al_2O_3$ was selected due to its prominent use as a high surface area support material in plasma catalysis. Neither material improved the measured CWG and the bimetallic catalyst reduced the CWG by 16% (Table 4). Both $\gamma$-$Al_2O_3$ and $Ni_4Fe/Al_2O_3$ resulted in lower $CH_4$ and $CO_2$ conversion than without catalyst, though the $Ni_4Fe$ bimetallic catalyst had a slightly higher $CH_4$ conversion than the $\gamma$-$Al_2O_3$ support alone (Fig. S7, ESI†). TEM images of each catalyst before and after experiments are shown in Fig. S8 (ESI†). Agglomeration of the $Ni_4Fe$ was not observed under TEM. Previous use of $Ni_4Fe$ catalysts for DRM has relied on higher temperatures (650 °C) while the heat generated by the plasma raised the bulk gas temperature to around 200 °C. Therefore, it is possible that $Ni_4Fe/Al_2O_3$ was significantly less active at these lower operating temperatures.

## Conclusions

In this work, we have demonstrated the coupling of plasma-assisted DRM for CNF formation in a tandem reactor. Increasing the power input to 12 W and increasing the plasma zone length to 11 cm resulted in the largest increases in CNF growth with an 87% and 106% increase in CWG, respectively. Lowering the total flow rate to 5 mL min$^{-1}$, without increasing the energy input, was also observed to increase CNF growth. Two catalysts, $\gamma$-$Al_2O_3$ and $Ni_4Fe/Al_2O_3$, did not play a role in increasing CNF growth in the current tandem setup. Using a plasma catalyst that can promote DRM and remain active at near-atmospheric temperatures may prove to enhance CNF formation from biogas in the future. In the current work we provided experimental results regarding the effects of the total flow rate of the biogas, the $CO_2/CH_4$ ratio in the feed, the plasma zone length, and the plasma power on CNF synthesis from biogas. Future studies on theoretical modeling of plasma processes are needed for the mechanistic understanding of CNF growth using the plasma-thermocatalytic tandem reactor.

## Data availability

The data supporting this article have been included as part of the ESI.†

## Conflicts of interest

There are no conflicts to declare.

## Acknowledgements

This work was financially supported by the Division of Chemical Sciences, Geosciences, & Biosciences, Office of Basic Energy Sciences, Department of Energy, under contract number DE-SC0012704 (BNL FWP CO-040). TEM measurements were performed using facilities at Center for Functional Nanomaterials (CFN) at Brookhaven National Laboratory under Contract No. DE-SC0012704. Kevin K. Turaczy also acknowledges support by the National Science Foundation Graduate Research Fellowship under Grant No. DGE 2036197.

## References

1 Intergovernmental Panel on Climate Change, Climate Change 2013: The Physical Science Basis. Contribution of Working Group I to the Fifth Assessment Report of the Intergovernmental Panel on Climate Change, 2013.
2 International Energy Agency, Outlook for biogas and biomethane: Prospects for organic growth, 2020.
3 A. I. Adnan, M. Y. Ong, S. Nomanbhay, K. W. Chew and P. L. Show, Technologies for Biogas Upgrading to Biomethane: A Review, *Bioengineering*, 2019, **6**, 92.
4 K. P. Loh, D. Ho, G. N. C. Chiu, D. T. Leong, G. Pastorin and E. K. H. Chow, Clinical Applications of Carbon Nanomaterials in Diagnostics and Therapy, *Adv. Mater.*, 2018, **30**, 1802386.
5 A. Mukherjee, S. Majumdar, A. D. Servin, L. Pagano, O. P. Dhankher and J. C. White, Carbon Nanomaterials in Agriculture: A Critical Review, *Front. Plant Sci.*, 2016, **7**, DOI: 10.3389/fpls.2016.00172.
6 R. K. Thines, N. M. Mubarak, S. Nizamuddin, J. N. Sahu, E. C. Abdullah and P. Ganesan, Application potential of carbon nanomaterials in water and wastewater treatment: A review, *J. Taiwan Inst. Chem. Eng.*, 2017, **72**, 116–133.

7 E. Hammel, X. Tang, M. Trampert, T. Schmitt, K. Mauthner, A. Eder and P. Pötschke, Carbon nanofibers for composite applications, *Carbon*, 2004, **42**, 1153–1158.
8 D. Sebastián, I. Suelves, R. Moliner, M. J. Lázaro, A. Stassi, V. Baglio and A. S. Aricó, Optimizing the synthesis of carbon nanofiber based electrocatalysts for fuel cells, *Appl. Catal., B*, 2013, **132–133**, 22–27.
9 Y. Yürüm, A. Taralp and T. N. Veziroglu, Storage of hydrogen in nanostructured carbon materials, *Int. J. Hydrogen Energy*, 2009, **34**, 3784–3798.
10 Z. Liu, D. Fu, F. Liu, G. Han, C. Liu, Y. Chang, Y. Xiao, M. Li and S. Li, Mesoporous carbon nanofibers with large cage-like pores activated by tin dioxide and their use in super-capacitor and catalyst support, *Carbon*, 2014, **70**, 295–307.
11 Z. Yu, Ø. Borg, B. C. Enger, V. Frøseth, E. Rytter, H. Wigum and A. Holmen, Carbon Nanofiber Supported Cobalt Catalysts for Fischer–Tropsch Synthesis with High Activity and Selectivity, *Catal. Lett.*, 2006, **109**, 43–47.
12 J. A. Díaz, M. Martínez-Fernández, A. Romero and J. L. Valverde, Synthesis of carbon nanofibers supported cobalt catalysts for Fischer–Tropsch process, *Fuel*, 2013, **111**, 422–429.
13 J. L. Pinilla, S. de Llobet, R. Moliner and I. Suelves, H2-rich gases production from Catalytic Decomposition of Biogas: Viability of the process associated to the co-production of carbon nanofibers, *Int. J. Hydrogen Energy*, 2017, **42**, 23484–23493.
14 J. L. Pinilla, S. de Llobet, R. Moliner and I. Suelves, Ni–Co bimetallic catalysts for the simultaneous production of carbon nanofibres and syngas through biogas decomposition, *Appl. Catal., B*, 2017, **200**, 255–264.
15 S. Saconsint, N. Sae-tang, A. Srifa, W. Koo-Amornpattana, S. Assabumrungrat, C. Fukuhara and S. Ratchahat, Development of high-performance nickel-based catalysts for production of hydrogen and carbon nanotubes from biogas, *Sci. Rep.*, 2022, **12**, 15195.
16 Z. Xie, E. Huang, K. K. Turaczy, S. Garg, S. Hwang, P. R. Kasala, P. Liu and J. G. Chen, ''Biogas sequestration to carbon nanofibers via tandem catalytic strategies'', *Nat. Chem. Eng.*, 2025, **2**, 118–129.
17 S. Garg, Z. Xie and J. G. Chen, Tandem reactors and reactions for $CO_2$ conversion, *Nat. Chem. Eng.*, 2024, **1**, 139–148.
18 Z. Xie, E. Huang, S. Garg, S. Hwang, P. Liu and J. G. Chen, $CO_2$ fixation into carbon nanofibres using electrochemical–thermochemical tandem catalysis, *Nat. Catal.*, 2024, **7**, 98–109.
19 A. N. Biswas, L. R. Winter, B. Loenders, Z. Xie, A. Bogaerts and J. G. Chen, Oxygenate Production from Plasma-Activated Reaction of $CO_2$ and Ethane, *ACS Energy Lett.*, 2022, **7**, 236–241.
20 R. Vertongen, G. De Felice, H. van den Bogaard, F. Galluci, A. Bogaers and S. Li, Sorption-Enhanced Dry Reforming of Methane in a DBD Plasma Reactor for Single-Stage Carbon Capture and Utilization, *ACS Sustainable Chem. Eng.*, 2024, **12**, 10841–10853.
21 I. Michielsen, Y. Uytdenhouwen, A. Bogaerts and V. Meynen, Altering Conversion and Product Selectivity of Dry Reforming of Methane in a Dielectric Barrier Discharge by Changing the Dielectric Packing Material, *Catalysts*, 2019, **9**, 51.
22 S. Liu, L. R. Winter and J. G. Chen, Review of Plasma-Assisted Catalysis for Selective Generation of Oxygenates from $CO_2$ and $CH_4$, *ACS Catal.*, 2020, **10**, 2855–2871.
23 L. R. Winter and J. G. Chen, Challenges and opportunities in plasma-activated reactions of $CO_2$ with light alkanes, *J. Energy Chem.*, 2023, **84**, 424–427.
24 C. De Bie, J. van Dijk and A. Bogaerts, The Dominant Pathways for the Conversion of Methane into Oxygenates and Syngas in an Atmospheric Pressure Dielectric Barrier Discharge, *J. Phys. Chem. C*, 2015, **119**, 22331–22350.
25 A. Bogaerts and R. Snoeckx, *An Economy Based on Carbon Dioxide and Water*, Springer, 2019, pp. 287–325.
26 R. Snoeckx, Y. X. Zeng, X. Tu and A. Bogaerts, Plasma-based dry reforming: improving the conversion and energy efficiency in a dielectric barrier discharge, *RSC Adv.*, 2015, **5**, 29799–29808.
27 J. Kim, D. B. Go and J. C. Hicks, Synergistic effects of plasma–catalyst interactions for CH4 activation, *Phys. Chem. Chem. Phys.*, 2017, **19**, 13010–13021.
28 M. M. B. Quiroga and A. E. C. Luna, Kinetic Analysis of Rate Data for Dry Reforming of Methane, *Ind. Eng. Chem. Res.*, 2007, **46**, 5265–5270.
29 D. H. Mei, S. Y. Liu and X. Tu, $CO_2$ reforming with methane for syngas production using a dielectric barrier discharge plasma coupled with Ni/$\gamma$-$Al_2O_3$ catalysts: Process optimization through response surface methodology, *J. $CO_2$ Util.*, 2017, **21**, 314–326.
30 L. Smoláková, M. Kout, L. Čapek, A. Rodriguez-Gomez, V. M. Gonzalez-Delacruz, L. Hromádko and A. Caballero, Nickel catalyst with outstanding activity in the DRM reaction prepared by high temperature calcination treatment, *Int. J. Hydrogen Energy*, 2016, **41**, 8459–8469.
31 S. Kawi, Y. Kathiraser, J. Ni, U. Oemar, Z. Li and E. T. Saw, Progress in Synthesis of Highly Active and Stable Nickel-Based Catalysts for Carbon Dioxide Reforming of Methane, *ChemSusChem*, 2015, **8**, 3556–3575.
32 S. M. Kim, P. M. Abdala, T. Margossian, D. Hosseini, L. Foppa, A. Armutlulu, W. van Beek, A. Comas-Vives, C. Copéret and C. Müller, Cooperativity and Dynamics Increase the Performance of NiFe Dry Reforming Catalysts, *J. Am. Chem. Soc.*, 2017, **139**, 1937–1949.